JFM RAPIDS
journals.cambridge.org/rapids

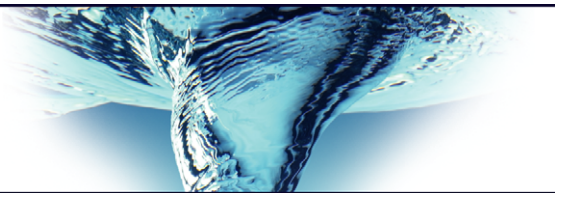

Magnetic-field effect on thermal convection of a nematic liquid crystal at large Rayleigh numbers

Stephan Weiss‡ and Guenter Ahlers†

Department of Physics, University of California, Santa Barbara, CA 93106, USA

(Received 2 August 2012; revised 8 October 2012; accepted 16 November 2012)

We report on near-turbulent thermal convection of a nematic liquid crystal heated from below in a cylindrical cell with an aspect ratio (diameter/height) equal to 0.50 for Rayleigh numbers $2 \times 10^7 \lesssim Ra \lesssim 3 \times 10^8$ and a Prandtl number of about 355. The Nusselt number Nu as a function of Ra did not differ significantly from that of an isotropic fluid. In a vertical magnetic field $\boldsymbol{H}$, we found $Nu(H)/Nu(0) = 1 + a(Ra)H^2$, with $a(Ra) = 0.24Ra^{0.75}$ G^{-2}. We present a model that describes the H dependence in terms of a change of the thermal conductivity in the thermal boundary layers due to a field-induced director alignment.

Key words: buoyant boundary layers, Bénard convection, liquid crystals

1. Introduction

In the study of thermal convection, experiments and simulations have focused primarily on isotropic Newtonian fluids that are confined by a warm horizontal plate from below and a colder parallel plate at a distance L from above (Rayleigh–Bénard convection (RBC)) – for reviews addressing a broad audience, see Kadanoff (2001) and Ahlers (2009), and for more specialized reviews, see Ahlers, Grossmann & Lohse (2009) and Lohse & Xia (2010). However, recently a significant interest has developed in turbulent convection of *complex* fluids, including, for instance, dilute polymer solutions (Ahlers & Nikolaenko 2010; Benzi, Ching & De Angelis 2010; Boffetta *et al.* 2010; Benzi, Ching & Chu 2011; Wei, Ni & Xia 2012) and nano-fluids (Ni, Zhou & Xia 2011). Here we contribute to this emerging field by reporting on RBC of a nematic liquid crystal (NLC) (Chandrasekhar 1992; Khoo 2007) at large Rayleigh numbers and on the effect of a vertical magnetic field $\boldsymbol{H}$ upon this system. It turns out that the field enhances the heat transport. We were able to describe this enhancement in terms of the field-induced preferred orientation of the NLC molecules in the thermal boundary layers (BLs) adjacent to the top and bottom confining plates.

† Email address for correspondence: guenter@physics.ucsb.edu

‡ Current address: Department of Physics & Center for the Study of Complex Systems, University of Michigan, Ann Arbor, MI 48109, USA.

doi:10.1017/jfm.2012.570

An NLC consists of elongated or discoidal molecules, which, primarily due to steric hindrance, tend to align their long axes locally relative to each other (see e.g. Chandrasekhar 1992). The local alignment direction is described by a director field $\hat{n}$. An NLC is Newtonian in the sense that its viscosities are independent of the applied shear, but it is anisotropic, and many of its properties, including the thermal conductivity λ, depend on the orientation of $\hat{n}$ relative to the direction of measurement. The conductivity $\lambda_\parallel$ parallel to $\hat{n}$, for instance, is larger than $\lambda_\perp$ perpendicular to $\hat{n}$ (Ahlers *et al.* 1994; Ahlers 1995). In the presence of $\boldsymbol{H}$, the director tends to align in the direction of $\boldsymbol{H}$ because of the anisotropy of the diamagnetic susceptibility. For $H = 0$ we found that the heat transport by turbulent RBC does not differ noticeably from that of an isotropic fluid. This is not surprising, given the stirring effect of the turbulent flow and the large cell dimensions in comparison to the short length scale of the spontaneous local ordering of the fluid molecules – which occurs on lengths of the order of a micrometre (see e.g. Khoo 2007). However, when a vertical magnetic field was applied, an increase of the heat transport was observed. We propose a model that describes this enhancement in terms of an increase of the thermal conductivity inside the thermal BLs due to a partial alignment of the director parallel to the magnetic field. Thus, this work also helps to illuminate the role of boundary layers in the heat transport by turbulent RBC.

We note that the thermal boundary layer is significantly thinner than and well embedded in the viscous boundary layer (see e.g. Ahlers *et al.* 2009). This is so because the kinematic viscosity of the liquid crystal used here is much larger than the thermal diffusivity. Thus, the stability of the thermal boundary layer and the plume emission rate are decoupled from the turbulent fluid in the bulk and only depend on the thermal gradient close to the plates.

There are a number of publications on chaotic patterns that occur in electro-hydrodynamic convection of NLCs (see e.g. Kai *et al.* 1990; Kai, i Hayashi & Hidaka 1996; Hidaka *et al.* 1997; Park, Clark & Noble 2005; Zhou & Ahlers 2006). In the experiments presented there, an alternating voltage is applied to a thin layer of the NLC. Above a certain threshold voltage, the director field can become chaotic in space and time for certain parameter ranges. These states have been referred to by some as 'phase turbulence' or 'soft-mode turbulence'. Notwithstanding this terminology, these states are *not* turbulent in the usual fluid-mechanical sense and are described more appropriately as 'spatio-temporal chaos'. Even though the director field is coupled to the velocity field, the velocity field is laminar and there is no energy cascade with a well-defined energy spectrum. Thus, this phenomenon has no relationship to the problem reported on in our present paper. A number of papers have also been published on the interesting topic of Rayleigh–Bénard convection in nematics near onset (for a review, see Ahlers 1995). However, to our knowledge, there are no previous publications that investigate how a nematic liquid crystal behaves in a hydrodynamically turbulent (or near-turbulent) flow that exists at larger Rayleigh numbers, i.e. a flow where energy is injected on a large scale and dissipated on a smaller scale.

From the values for the Rayleigh number Ra, the Prandtl number Pr and the Nusselt number Nu (all to be defined explicitly below in § 2), we can calculate a volume-averaged coherence length $l/L \approx 10Pr^{1/2}/[(Nu-1)^{1/4}Ra^{1/4}]$ (see e.g. Grossmann & Lohse 1993). This length describes the largest coherent structure that is expected to prevail in the system, and the system is considered 'turbulent' when l/L is well below unity. For our sample one finds $l/L \simeq 1.26$ for the smallest Ra ($Ra = 2.5 \times 10^7$) and $l/L \simeq 0.59$ for the largest Ra. Thus, for the smallest Ra, one expects that the flow did

not really lose its coherence over the height of the cell and should not be considered turbulent. For the largest Ra, the flow reached a small degree of turbulence. Clearly a study at larger values of Ra (and thus smaller l/L) would have been desirable. However, this could be achieved only by increasing L, and at constant aspect ratio the fluid volume would increase as L^3. The fluid contained in our sample (which had a volume of about 1400 cm^3) was acquired at a cost of about \$5000. Decreasing l/L by a factor of 2, for instance, would require an increase of Ra (and the fluid volume) by about a factor of 8, leading to a cost of about \$40 000 for the fluid. One sees that there is a practical limit to the maximum Ra and minimum l/L values accessible to experiments in this field.

The remainder of this paper is organized as follows. In § 2 we define the parameters relevant to this system. Then, in § 3, we give a brief description of the apparatus used for the measurements. The results in the absence of a field are presented in § 4, and those for $H > 0$ are discussed in § 5. The boundary-layer model that describes our experimental findings is explained in § 6, and a brief summary of the work is given in § 7.

2. Relevant parameters

For isotropic Newtonian fluids and a given sample geometry, the state of the system depends on two dimensionless variables. The first is the Rayleigh number Ra, a dimensionless form of the temperature difference $\Delta T = T_b - T_t$ between the bottom (T_b) and the top (T_t) plate. It is given by

$$Ra = \frac{g\alpha \Delta T L^3}{\kappa \nu}. \tag{2.1}$$

Here, g, α, κ and ν denote the gravitational acceleration, the isobaric thermal expansion coefficient, the thermal diffusivity and the kinematic viscosity, respectively. The second is the Prandtl number $Pr = \nu/\kappa$. For the NLC one needs to use $\nu = \alpha_4/2\rho$, where α_4 is the fourth Leslie coefficient (see e.g. Ahlers 1995) and ρ is the density. The vertical heat transport from the bottom to the top plate is expressed in dimensionless form by the Nusselt number

$$Nu = \frac{\lambda_{eff}}{\lambda}, \tag{2.2}$$

where

$$\lambda_{eff} = QL/(A\Delta T) \tag{2.3}$$

and where Q is the heat flux and A is the cross-sectional area of the cell.

3. Apparatus and procedure

The experiments presented here were conducted using the NLC 4-cyano-4′-pentylbiphenyl (5CB) at a mean temperature $T_m = (T_b + T_t)/2 = 27.00$ °C where $Pr = 355$. Even for the measurements with the largest temperature difference, the bottom-plate temperature was significantly lower than the clearing-point temperature $T_{NI} = 35.2$ °C. The relevant fluid properties were compiled by Ahlers (1995). We used the 'small convection apparatus' (SCA) described in detail by Weiss & Ahlers (2011). A cylindrical sample cell with $L = 190.5$ mm and a circular cross-section of diameter $D = 95.3$ mm, giving an aspect ratio $\Gamma = D/L = 0.500$, was used. It was confined by

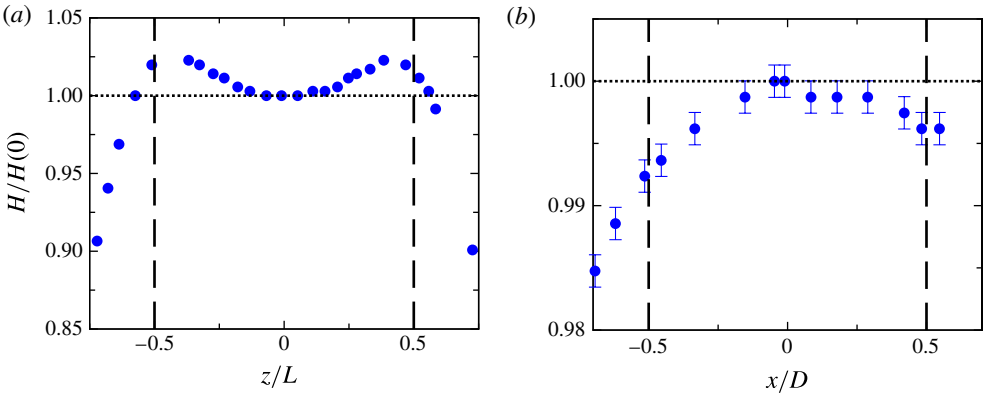

FIGURE 1. (*a*) The normalized magnetic field magnitude $H/H(z/L = 0)$ along the vertical axis of the solenoid. Measurement errors are smaller than the symbol size, and $H(0) = 353$ G. (*b*) The normalized magnetic field magnitude $H/H(x/D = 0)$ along the diameter at the mid-height of the solenoid. For these measurements, $H(0) = 78.7$ G. In both panels, the vertical dashed lines denote the boundaries of the sample.

thick copper plates from below and above, and had a 3.2 mm thick sidewall made of Lexan. The bottom plate was heated by a film heater from below and the top plate was in thermal contact with a temperature-controlled circulating water bath. Each of the two copper plates was equipped with two thermistors for precise temperature measurements. In contrast to convection experiments in smaller cells (Ahlers 1995), the surfaces of the top and bottom plate were not treated in order to align the director in a specific direction. The directors at the top and bottom boundaries are therefore expected to be randomly distributed. In any event, surface director alignment would not have a significant influence in a sample as large as ours.

As described by Weiss & Ahlers (2011) (see especially figure 1 therein), the convection cell was located in an air- and foam-filled container, which in turn was surrounded by cooling water for the top plate at a temperature nearly equal to T_t. Even though the cell was insulated, there was still a small but significant heat loss from the sidewall and the bottom plate to the container. This heat loss, together with the conduction through the sidewall, was measured while the cell was filled with air and foam. For the measurements of *Nu*, it was subtracted from the heat input to the bottom plate.

Only non-ferromagnetic materials were used to build the apparatus in order to avoid disturbances of the magnetic field. Four coils, designed to provide an exceptionally homogeneous field over a large volume, surrounded the main apparatus and were used to generate a vertical field. Their axes coincided with the axis of the convection cell and their vertical positions were such that the centre of the field coincided with the horizontal mid-plane of the sample cell. We used a gaussmeter (Lakeshore, 421) with two different Hall probes (Lakeshore, MMT-6J08-VH and MMA-2508-VH) in order to measure the magnetic field variation in the vertical (i.e. along the cylinder axis) and in the radial direction (i.e. vertical to the cylinder axis). These measurements were done for the empty magnet, i.e. without the convection apparatus present. While measurements along the cylinder axis were straightforward, a small hole at mid-height

between the magnetic coils was used in order to introduce the Hall probe from the side and thus measure the radial dependence of the magnetic field. Figure 1(*a*) shows the magnetic field magnitude H along the cylinder axis of the cell. The vertical dashed lines mark the locations of the top and bottom plates. As shown, there is a small variation of H along the z-axis, so that at $z = 0$, H is approximately 2 % smaller than at the top and bottom plates. The variation of H in the horizontal direction at $z = 0$ is shown in figure 1(*b*). There H was slightly higher in the middle of the cell than at the sidewall. However, the variation was less than 1 %. Overall, we do not expect the small field inhomogeneity to have a significant effect on the outcome of the measurements.

During a typical experimental run, the temperatures of the top and bottom plates were held constant and the power dissipated at the bottom plate was measured. The temperature of all thermistors as well as the power were recorded every 4 s for about 24 h.

4. Results for the Nusselt number in the absence of a magnetic field

First we measured Nu as a function of Ra for $H = 0$. Without field alignment, a coherent director would exist only over a length of the order of a micrometre or so (Chandrasekhar 1992; Khoo 2007), which is much smaller than any length scales of the system. We note that the thermal BL thickness was about 2 mm for the largest Nu and thus $\sim 10^3$ times larger than the distance over which molecules were aligned in the absence of a field. Thus, we assumed that $\hat{n}$ was randomly distributed throughout the sample, and computed Ra and Nu as defined by (2.1) and (2.2) using averaged values,

$$\lambda_0 \equiv (2\lambda_\perp + \lambda_\parallel)/3 \tag{4.1}$$

and $\kappa = \lambda_0/\rho c_p$. Here c_p is the heat capacity at constant pressure per unit mass. The data were corrected for the heat flux through the sidewall. By using model 2 of Ahlers (2000), the large thermal gradients in the sidewall but close to the thermal boundary layers in the fluid were taken into consideration.

Figure 2(*a*) shows Nu as a function of Ra for 5CB (solid circles, red online) on a double logarithmic plot. In order to display more detail, the reduced Nusselt number $Nu/Ra^{0.3}$ is plotted on a linear scale as a function of Ra on a logarithmic scale in figure 2(*b*). A fit of the power law $Nu \propto Ra^{\gamma_{eff}}$ to the data gave $\gamma_{eff} = 0.309$, which is in excellent agreement with the effective exponent $\gamma_{eff}^{GL} = 0.307$ derived from the Grossmann–Lohse (GL) model (Grossmann & Lohse 2001) (dotted line) for this Pr and the same Ra range. For comparison, we show data for isotropic fluids with $Pr = 205$ (open circles, green online) and $Pr = 396$ (open squares, purple online) from Xia *et al.* (2002). Inspection of figure 2(*b*) shows that they are consistent with the $\gamma_{eff} = 0.309$ of the 5CB data. The differences by a few per cent between the various data sets and the GL model at the same Ra can be attributed in part to the differences of Pr and Γ, and in part to systematic errors in the fluid properties and the sidewall corrections (Ahlers 2000). Thus, as expected, we conclude that there is no measurable difference between $Nu(Ra)$ for the isotropic fluids and the anisotropic NLC when the average conductivity given by (4.1) is used to evaluate Nu and Ra.

In the next section we only present measurements for which $l/L \lesssim 1$. We note also that in the chaotic regime just below the turbulent state (see, for instance, the supplementary material provided by Bosbach, Weiss & Ahlers (2012)) there is vigorous mixing in the sample interior, and the boundary layers central to our discussion already exist.

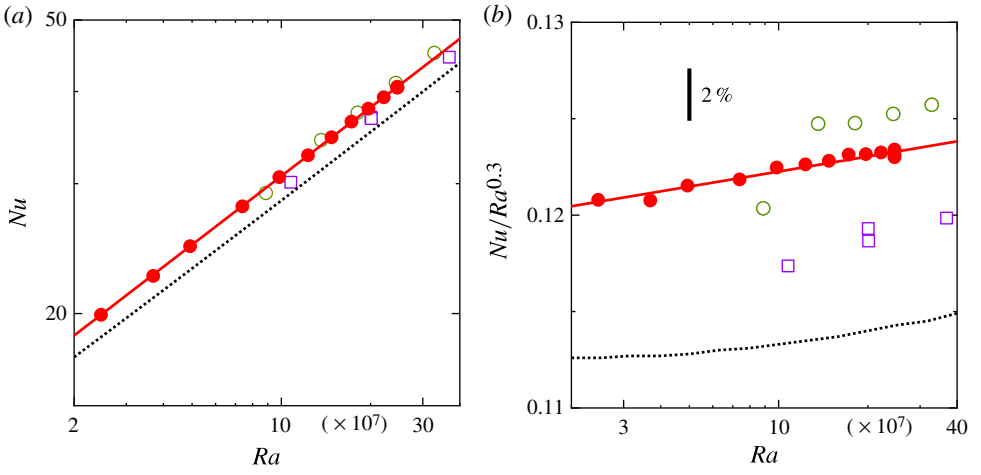

FIGURE 2. (*a*) The Nusselt number as a function of the Rayleigh number on logarithmic scales. (*b*) The reduced Nusselt number $Nu/Ra^{0.3}$ on a linear scale as a function of Ra on a logarithmic scale. Solid circles (red online): this work, 5CB, $Pr = 355$, $\Gamma = 0.50$. Open squares (purple online): Xia, Lam & Zhou (2002), $Pr = 396$, $\Gamma = 1.00$. Open circles (green online): Xia *et al.* (2002), $Pr = 205$, $\Gamma = 1.00$. Solid line (red online): the power-law fit to the 5CB data, which gave $Nu = 0.103Ra^{0.309}$. Dotted line: Grossmann–Lohse model (Grossmann & Lohse 2001) for $Pr = 355$ and $\Gamma = 1$.

5. Effect of a magnetic field on the heat transport

In a second set of experiments we applied a vertical magnetic field and studied its influence on the heat transport. The field has an influence on the director alignment and thus on the fluid properties, in particular on λ and κ. Owing to the dependence of Ra and Nu on these properties, they are no longer useful as control and response parameters. Instead, we used the effective thermal conductivity λ_{eff} as defined by (2.3) as a measure for the heat transport and

$$R_0 = \frac{\alpha g \rho c_p L^3 \Delta T}{\lambda_0 \nu} \tag{5.1}$$

as the control parameter (the dimensionless temperature difference). We then have $Ra = R_0\,\lambda_0/\lambda$.

Figure 3(*a*) shows the normalized effective heat conductivity $\lambda_{eff}(H)/\lambda_{eff}(0)$ for different R_0. One sees that $\lambda_{eff}(H)$ increases with H. The relative increase $\lambda_{eff}(H)/\lambda_{eff}(0)$ at a given H is largest for the smallest R_0. In order to quantify the relative increase, we fit the parabola

$$\frac{\lambda_{eff}(H)}{\lambda_{eff}(0)} = 1 + aH^2 \tag{5.2}$$

to the data points with the coefficient $a(R_0)$ depending only on R_0. In figure 3(*b*) we plot $a(R_0)$ versus R_0. The data can be represented by a simple power law

$$a = mR_0^n \tag{5.3}$$

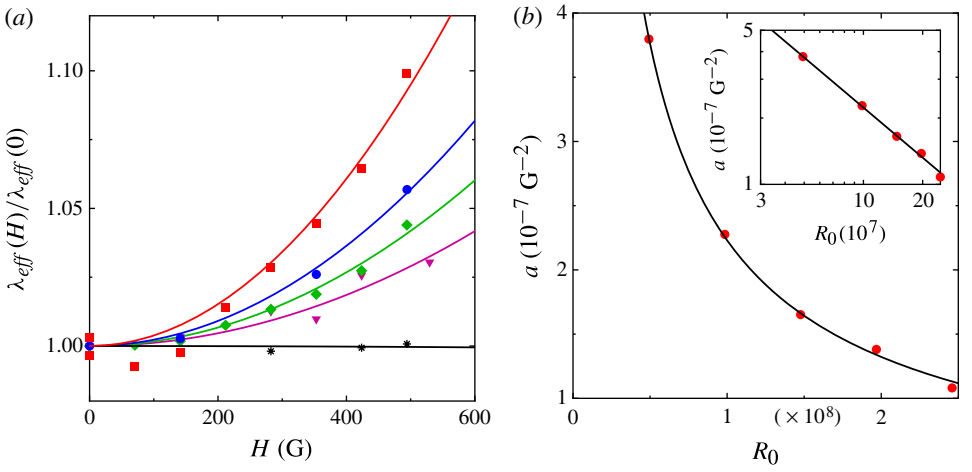

FIGURE 3. (*a*) Reduced thermal conductivity $\lambda_{eff}(H)/\lambda_{eff}(0)$ as a function of the applied magnetic field H for $R_0 = 4.9 \times 10^7$ (squares, red online), 9.8×10^7 (bullets, blue online), 1.5×10^8 (diamonds, green online), and 2.5×10^8 (triangles, purple online). The black stars are for the isotropic phase ($T_m = 40.00\,^{\circ}$C) and $R_0 = 2.8 \times 10^8$. Solid lines are fits of (5.3). (*b*) Fitting parameter a as a function of R_0. The solid line shows the power law $a = mR_0^n$ with $m = 0.24$ G^{-2} and $n = -0.75$ (the inset shows the same data on double logarithmic scales).

with $m = 0.24 \pm 0.06$ G^{-2} and $n = -0.75 \pm 0.01$. In the remainder of this article, we show that the above experimental findings can be fitted well by a simple model of the thermal BLs.

6. A simple model for the magnetic-field effect

In RBC at large Ra one can distinguish a bulk region where, due to turbulent mixing, the vertical temperature gradient nearly vanishes in the time average (see, however, Tilgner, Belmonte & Libchaber 1993; Brown & Ahlers 2007; Ahlers *et al.* 2012), and thermal BLs with large vertical thermal gradients. A simple model (Malkus 1954; Zocchi, Moses & Libchaber 1990) assumes that the temperature gradient really vanishes in the bulk, and that half of ΔT is sustained over each of the BLs. It is assumed that the heat transport within the BLs is by conduction only, and that the BLs adjust their thickness δ so that they are marginally stable. Since the heat flux through the BLs is equal to the flux from the bottom to the top of the cell, one has

$$\lambda_{eff}\frac{\Delta T}{L} = \lambda\frac{\Delta T}{2\delta} \tag{6.1}$$

and thus

$$\lambda_{eff} = \lambda\frac{L}{2\delta}. \tag{6.2}$$

In the following we extend this model to describe the behaviour of $\lambda_{eff}(H)/\lambda_{eff}(0)$ as a function of H and R_0 in terms of the change of the ordering of the director and of the associated change of the thermal conductivity $\lambda(H)$ in the thermal BLs due to the applied magnetic field.

Since δ corresponds to marginal stability of the BLs, it can be expressed in terms of a critical Rayleigh number $Ra_c^{BL} = g\alpha(\Delta T/2)\delta^3/(\kappa\nu)$ for the BLs by

$$\delta = \left(\frac{Ra_c^{BL}\nu}{g\alpha c_p \rho}\,\frac{2\lambda}{\Delta T}\right)^{1/3} \tag{6.3}$$

$$= L\left(\frac{Ra_c^{BL}}{R_0}\,\frac{2\lambda}{\lambda_0}\right)^{1/3}. \tag{6.4}$$

The exact value of Ra_c^{BL} is not important for the further analysis; it only matters that it is a constant. The assumption of a constant Ra_c^{BL} leads to $Nu \propto Ra^{1/3}$, which differs slightly from the experimental result $Nu \propto Ra^{0.309}$. This small difference is of little consequence for the model, and using a constant Ra_c^{BL} makes the model simpler and conceptually more appealing. Substituting (6.4) into (6.1) gives

$$\lambda_{eff} = \left(\frac{1}{2}\right)^{4/3}\left(\frac{R_0\lambda_0}{Ra_c^{BL}}\right)^{1/3}\lambda^{2/3}. \tag{6.5}$$

The thermal conductivity $\lambda(H)$ in the BLs is unknown since it depends on the extent of the alignment of $\hat{n}$ in the BLs by H. For very large H, the director will be aligned parallel to the magnetic field and thus $\lim_{H\to\infty}\lambda(H) = \lambda_\parallel$. As we argued above, and as is borne out by the zero-field measurements of $Nu(Ra)$, without a magnetic field the director is randomly distributed and thus $\lambda(H=0) = \lambda_0$. It is reasonable to assume that λ depends not only on H but also on the dimensionless temperature difference R_0. In fact, for large R_0 the flow is more turbulent, which disturbs the magnetic-field-induced director alignment in the thermal boundary layers due to an applied shear and an increase in the plume emission rate. Therefore we consider λ as a function of the ratio H/R_0^b, with b an unknown exponent.

We write the BL conductivity as

$$\lambda(x) = \lambda_0 + (\lambda_\parallel - \lambda_0)f(x) \tag{6.6}$$

with

$$x = \left(\frac{H/H_0}{R_0^b}\right)^2. \tag{6.7}$$

Here $f(x)$ is a convenient cross-over function, with $f(x=0) = 0$ and $\lim_{x\to\infty} f(x) = 1$, and H_0 sets the scale of H. We choose

$$f(x) = \frac{x^2 + x}{x^2 + x + 1}, \tag{6.8}$$

but that choice is of minor importance. Substituting $\lambda(x)$ into (6.5) and dividing by $\lambda_{eff}(x=0)$ one gets

$$\frac{\lambda_{eff}(x)}{\lambda_{eff}(0)} = [1 + (\lambda_\parallel/\lambda_0 - 1)f(x)]^{2/3}. \tag{6.9}$$

For small x, a Taylor expansion of (6.9) yields

$$\frac{\lambda_{eff}(H)}{\lambda_{eff}(0)} = 1 + \frac{2}{3}(\lambda_\parallel/\lambda_0 - 1)x + \mathscr{O}(x^2) \tag{6.10}$$

$$\approx 1 + \frac{2}{3}\left(\frac{\lambda_\parallel}{\lambda_0} - 1\right)\left(\frac{H/H_0}{R_0^b}\right)^2. \tag{6.11}$$

Equation (6.11) is the same as (5.2) if we set $a = (2/3)(\lambda_\parallel/\lambda_0 - 1)H_0^{-2}R_0^{-2b}$. Thus, the fit parameter m in (5.3) is a ratio of a material parameter to the square of the scale H_0 of H. It is given by

$$m = (2/3)(\lambda_\parallel/\lambda_0 - 1)/H_0^2 \tag{6.12}$$

$$= 0.243/H_0^2. \tag{6.13}$$

Comparison with the experimental values $m = 0.24\ \mathrm{G}^{-2}$ and $n = -2b = -0.75$ obtained from a fit to the experimental data in figure 2 indicates that $H_0 \simeq 1$ G and that $b = 0.375$. A fit of the full equation (equation (6.9) with (6.8)) to the data gives the exponent $2b = 0.751$, which shows that the lowest-order Taylor expansion (equation (6.11)) is an excellent approximation in our range of H.

As shown above, the exact form of the cross-over function $f(x)$ can vary. Since our data points only cover small values of x, other functions that can be approximated by a parabola for small x and asymptotically reach unity for large x are equally suitable. While possible alternative functions include $\tanh(x)$, $\mathrm{erf}(x)$ or $1 - \exp(-x)$, a ratio of two linear functions such as $x/(x + 1)$ provides only a poor fit since the second-order term of its Taylor expansion becomes important in the range of our data.

This model focuses on the change of the heat conductivity λ due to the applied magnetic field. One could ask whether the director orientation might also have an effect on the viscosity and thus on the momentum dissipation (see, for instance, Feng, Pesch & Kramer (1992) for a discussion of the equations of motion of this system). We believe that this is not the case because the Leslie viscosity coefficients do not depend on H, and because most of the momentum is dissipated in the bulk, where the director orientation is randomly distributed due to vigorous fluid motion, even when a magnetic field is present. In addition, almost the entire temperature gradient (which determines the Nusselt number) is in the thermal BLs, which for a large-Pr fluid like an NLC are deeply embedded in the viscous BLs where there is virtually no flow.

7. Summary

In this paper we have reported experimental results for turbulent thermal convection of a nematic liquid crystal in a vertical magnetic field of strength H. For $H = 0$ we found that the NLC behaved much like an isotropic fluid provided that the thermal conductivity used to calculate Ra and Nu was that of a sample with a random director orientation (see (4.1)). In the presence of a vertical magnetic field, the heat transport was enhanced. This increase was larger for smaller thermal driving (smaller temperature differences). We proposed a model that assumed an increase of the heat conductivity of the fluid in the thermal BLs due to a field-induced alignment of the director. By only considering the thermal BLs, the model reproduced the experimental data very well. A remaining challenge is an *a priori* calculation of the exponent $n = -2b \simeq 0.75$ and of the scale $H_0 \simeq 1$ G of the magnetic field.

We believe that this system is well suited for further studies of the properties of the thermal boundary layers since the properties of the fluid can easily be changed during an experiment by changing the applied field. Measurements in the presence of a horizontal field would also be of interest since our model is easily extended to this case. However, generating a sufficiently large and homogeneous horizontal field over the volume of the sample would be a significant undertaking.

Acknowledgement

This work was supported by the US National Science Foundation through Grant DMR11-58514.

References

AHLERS, G. 1995 *Experiments on Thermally Driven Convection*, pp. 165–220, Springer.

AHLERS, G. 2000 Effect of sidewall conductance on heat-transport measurements for turbulent Rayleigh–Bénard convection. *Phys. Rev.* E **63**, R015303.

AHLERS, G. 2009 Turbulent convection. *Physics* **2**, 74.

AHLERS, G., BODENSCHATZ, E., FUNFSCHILLING, D., GROSSMANN, S., HE, X., LOHSE, D., STEVENS, R. & VERZICCO, R. 2012 Logarithmic temperature profiles in turbulent Rayleigh–Bénard convection. *Phys. Rev. Lett.* **109**, 114501.

AHLERS, G., CANNELL, D. S., BERGE, L. I. & SAKURAI, S. 1994 Thermal conductivity of the nematic liquid crystal 4-n-pentyl-4′-cyanobiphenyl. *Phys. Rev.* E **49**, 545–553.

AHLERS, G., GROSSMANN, S. & LOHSE, D. 2009 Heat transfer and large-scale dynamics in turbulent Rayleigh–Bénard convection. *Rev. Mod. Phys.* **81**, 503–538.

AHLERS, G. & NIKOLAENKO, A. 2010 Effect of a polymer additive on heat transport in turbulent Rayleigh–Bénard convection. *Phys. Rev. Lett.* **104**, 034503.

BENZI, R., CHING, E. S. C. & CHU, V. W. S. 2011 Heat transport by laminar boundary layer flow with polymers. *J. Fluid Mech.* **696**, 330–344.

BENZI, R., CHING, E. S. C. & DE ANGELIS, E. 2010 Effect of polymer additives on heat transport in turbulent thermal convection. *Phys. Rev. Lett.* **104** (2), 024502.

BOFFETTA, G., MAZZINO, A., MUSACCHIO, S. & VOZELLA, L. 2010 Polymer heat transport enhancement in thermal convection: the case of Rayleigh–Taylor turbulence. *Phys. Rev. Lett.* **104**, 184501.

BOSBACH, J., WEISS, S. & AHLERS, G. 2012 Plume fragmentation by bulk interactions in turbulent Rayleigh–Bénard convection. *Phys. Rev. Lett.* **108**, 054501.

BROWN, E. & AHLERS, G. 2007 Temperature gradients, and search for non-Boussinesq effects, in the interior of turbulent Rayleigh–Bénard convection. *Europhys. Lett.* **80**, 14001.

CHANDRASEKHAR, S. 1992 *Liquid Crystals*. Cambridge University Press.

FENG, Q., PESCH, W. & KRAMER, L. 1992 Theory of Rayleigh–Bénard convection in planar nematic liquid crystals. *Phys. Rev.* A **45**, 7242–7256.

GROSSMANN, S. & LOHSE, D. 1993 Characteristic scales in Rayleigh–Bénard turbulence. *Phys. Lett.* A **173**, 58–62.

GROSSMANN, S. & LOHSE, D. 2001 Thermal convection for large Prandtl number. *Phys. Rev. Lett.* **86**, 3316–3319.

HIDAKA, Y., HUH, J., HAYASHI, K., KAI, S. & TRIBELSKY, M. 1997 Soft-mode turbulence in electrohydrodynamic convection of a homeotropically aligned nematic layer. *Phys. Rev.* E **56**, R6256–R6259.

KADANOFF, L. P. 2001 Turbulent heat flow: structures and scaling. *Phys. Today* **54** (8), 34–39.

KAI, S., HAYASHI, K. & HIDAKA, Y. 1996 Pattern forming instability in homeotropically aligned liquid crystals. *J. Phys. Chem.* **100**, 19007.

KAI, S., ZIMMERMANN, W., ANDOH, M. & CHIZUMI, N. 1990 Local transition to turbulence in electrohydrodynamic convection. *Phys. Rev. Lett.* **64**, 1111–1114.

KHOO, I.-C. 2007 *Liquid Crystals*. Wiley.

LOHSE, D. & XIA, K.-Q. 2010 Small-scale properties of turbulent Rayleigh–Bénard convection. *Annu. Rev. Fluid Mech.* **42**, 335–364.

MALKUS, M. V. R. 1954 The heat transport and spectrum of thermal turbulence. *Proc. R. Soc. Lond.* A **225**, 196–212.

NI, R., ZHOU, S.-Q. & XIA, K.-Q. 2011 An experimental investigation of turbulent thermal convection in water-based alumina nanofluid. *Phys. Fluids* **23**, 022005.

PARK, C., CLARK, N. & NOBLE, R. 2005 A convective turbulente state that spatially orders upon increased drive. *Phys. Fluids* **17**, 055101.

TILGNER, A., BELMONTE, A. & LIBCHABER, A. 1993 Temperature and velocity profiles of turbulence convection in water. *Phys. Rev.* E **47**, R2253–R2256.

WEI, P., NI, R. & XIA, K.-Q. 2012 Enhanced and reduced heat transport in turbulent thermal convection with polymer additives. *Phys. Rev.* E **86**, 016325.

WEISS, S. & AHLERS, G. 2011 Turbulent Rayleigh–Bénard convection in a cylindrical container with aspect ratio $\Gamma = 0.50$ and Prandtl number $Pr = 4.38$. *J. Fluid Mech.* **676**, 5–40.

XIA, K.-Q., LAM, S. & ZHOU, S. Q. 2002 Heat-flux measurement in high-Prandtl-number turbulent Rayleigh–Bénard convection. *Phys. Rev. Lett.* **88**, 064501.

ZHOU, S.-Q. & AHLERS, G. 2006 Spatio-temporal chaos in electro-convection of a homeotropically aligned nematic liquid crystal. *Phys. Rev.* E **74**, 046212.

ZOCCHI, G., MOSES, E. & LIBCHABER, A. 1990 Coherent structures in turbulent convection: an experimental study. *Physica* A **166**, 387–407.